UC Berkeley
UC Berkeley Previously Published Works

Title
Experimental and Theoretical Study of n-Butanal Self-Condensation over Ti Species Supported on Silica

Permalink
https://escholarship.org/uc/item/4zx912mn

Journal
ACS Catalysis, 4(9)

ISSN
2155-5435

Authors
Hanna, David G
Shylesh, Sankaranarayanapillai
Li, Yi-Pei
et al.

Publication Date
2014-09-05

DOI
10.1021/cs500704b

Peer reviewed

eScholarship.org Powered by the California Digital Library
University of California

I&EC research
Industrial & Engineering Chemistry Research

Article

Cite This: Ind. Eng. Chem. Res. 2018, 57, 2773−2786

pubs.acs.org/IECR

Experimental and Theoretical Study for Vapor Phase Aldol Condensation of Methyl Acetate and Formaldehyde over Alkali Metal Oxides Supported on SBA-15

Teng He, Yixin Qu, and Jidong Wang*

Beijing Key Laboratory of Membrane Science and Technology, College of Chemical Engineering, Beijing University of Chemical Technology, Beijing 100029, PR China

Supporting Information

ABSTRACT: Alkali metal oxides supported on SBA-15, M/SBA-15 (M = Li, Na, K, Rb, and Cs), prepared by the impregnation method were characterized and tested for the aldol condensation of methyl acetate and formaldehyde to methyl acrylate (MA). M/SBA-15 catalysts are active for the formation of MA while the support is inert. The supported alkali metals react with hydroxyl groups on SBA-15 by replacing the H atoms and generate weak and medium basic sites. The latter plays an important role in promoting the reaction. Coke formation results in deactivation of Cs/SBA-15, and the deactivated catalyst can be regenerated by burning off the coke. Two possible reaction pathways for the formation of MA were explored using quantum calculations. The predicated activity for M/SBA-15 is consistent with the experimental observations. A pathway with adsorbed enol molecule as an intermediate was suggested to be predominant for the formation of MA.

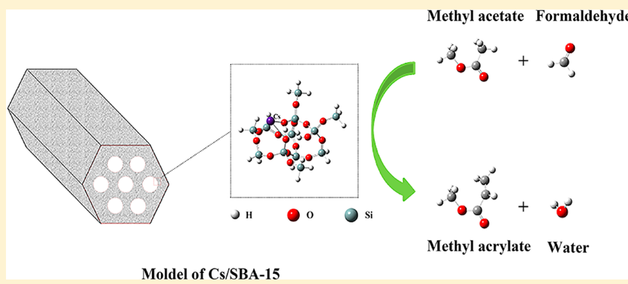

1. INTRODUCTION

Methyl acrylate (MA) is widely used in the manufacture of various resins and polymers. It is also a reagent in the synthesis of various pharmaceutical intermediates. Up to now, MA is mainly produced via the two-stage catalytic oxidation of propylene with air.[1] Since propylene is mainly derived from crude oil, its price is closely associated with that of crude oil. As the consumption of MA is expected to increase in the following years, new ways for the production of MA at lower cost are desired.

Methyl acetate (Ma) is a main byproduct in the preparation of purified terephthalic acid and poly(vinyl alcohol).[2] Besides using Ma as a solvent, finding new ways for the application of the byproduct Ma is always an attractive subject due to its relatively low price. In 1969, Fernholz and Wunder[3] disclosed a method for the preparation of MA by aldol condensation reaction of Ma and formaldehyde (FA). Considering that FA is also cheap and facile, it is a green method to use the byproduct Ma to produce the useful material MA.

There are two main kinds of catalysts used for vapor phase aldol condensation. The first kind mainly comprises vanadium phosphorus oxide catalysts.[4−9] The second kind is supported alkali metal oxides or alkaline earth metal oxides catalysts.[10−13] Besides, hydrotalcite-like material,[14] zeolite,[15] 12-tungstosilicic acid,[16] and ionic liquid[17] were also found to be active for this reaction.

Using V−P binary oxides, Ai[4,5] studied the effects of reaction conditions on the aldol condensation of FA with acetic acid (Aa) and propionic acid, respectively. In a further study, Ai[6] found that the combination of V−P oxide and Ti−P oxide could produce catalysts with large surface area and enhanced acidity, which contributed to the high activity of the V−Ti−P oxides. Subsequently, Ai[7] made a series of catalysts with a V−Ti−P atomic ratio of 1:2:*x* and found that the activity of catalysts with a fixed V/Ti atomic ratio of 1:2 was significantly influenced by the content of the third component, phosphorus. The highest yield of the aldol condensation products was obtained with a catalyst having an atomic ratio of P/V = 6.0. With this catalyst, the influence of reaction conditions on the catalytic performance was investigated.[8] Feng et al.[9] found that the activation conditions largely affect the composition and texture of V−P oxides.

Supported alkali metal oxides or alkaline earth metal oxide catalysts are usually prepared by the impregnation method. The condensation of methyl propionate with FA was studied by Ai[10] and Li et al.[11] Using silica-supported alkali and alkaline earth metal hydroxides as catalysts, Ai[10] found that cesium hydroxide supported on silica showed the highest selectivity. Li et al.[11] compared the catalytic performance of cesium oxides supported on SiO_2 and SBA-15 and found that with a similar Cs loading (ca. 15 wt %), the catalysts with SBA-15 as a support exhibited better selectivity. Yan et al.[12] used cesium supported on SBA-15 catalysts for the vapor phase aldol condensation of Ma and FA.

Received: July 11, 2017
Revised: January 11, 2018
Accepted: February 12, 2018
Published: February 12, 2018

Downloaded via UNIV OF CALIFORNIA BERKELEY on September 4, 2018 at 18:10:40 (UTC).
See https://pubs.acs.org/sharingguidelines for options on how to legitimately share published articles.

ACS Publications © 2018 American Chemical Society

On the basis of their study, they proposed that the Si−O−Cs species were the active sites for this reaction. Recently, Wang et al.[13] found the addition of a suitable amount of La and activation at appropriate conditions could promote the activity of Cs/SBA-15 catalysts.

In addition, other researchers[18−21] found that catalysts with acid−base bifunctional property showed better performance than the catalysts with only acid or base property. The catalysts with acid−base bifunctional property can be prepared by using a combination of appropriate active components. For example, Zhang et al.[18] used P-doped Cs oxide supported on γ-Al_2O_3 as catalysts and observed a high activity for the aldol condensation of Ma and FA, which was ascribed to the high density of weak acidic and weak basic sites on this material. Yang et al.[19,20] investigated the performance of V and P oxides supported on SiO_2 and found that the textural, acid−base property and the ratio of V^{4+} to V^{5+} were important in determining the activity of the catalysts. Using SiO_2, SBA-15, and HZSM-5 as supports for V−P oxides, Hu et al.[21] found that the support type and the P/V atomic ratio affect the acid−base property and the activity of these catalysts.

The CO_2-TPD technique is usually used to characterize the strength and the amount of basic sites of catalysts. Three modes for the adsorption of CO_2 at ambient temperature on alkali metal modified materials have been proposed[22−24] as shown in Scheme 1. The monodentate carbonate formation requires

Scheme 1. Modes of CO_2 Adsorption on Different Basic Sites

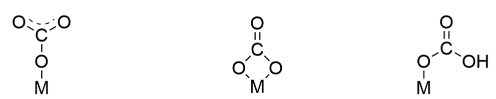

Monodentate carbonate   Bidentate carbonate   Bicarbonate

isolated surface O^{2-} ions. The bidentate carbonate forms on Lewis-acid-Brönsted-base pairs (M^{n+}-O^{2-} pair site). The bicarbonate species formation involves surface hydroxyl groups. It can be seen from these models that one basic site adsorbes one CO_2 molecule.[25]

The basic properties of alkali-promoted MgO catalysts were studied by Díez et al.[23] in terms of CO_2-TPD and IR techniques. Deconvolution of the CO_2-TPD profiles indicated that three types of basic sites can be distinguished on these catalysts. The weak basic sites with a desorption temperature of CO_2 at 373 K, the medium basic sites at 500 K, and the strong basic sites at 573 K. The IR spectra observed at different temperatures revealed that the weak basic sites could be ascribed to the bicarbonate adsorption model, the medium basic sites to the bidentate carbonate, and the strong basic sites to the monodentate carbonate.

In the previous studies, most of the works focused on elucidating the influence of preparation, composition, texture, and base or acid−base properties on the catalytic performance. Concerning the alkali metal oxide catalysts, the interaction of the alkali metals with the supports, the effect of the strength and density of the basic sites on the catalytic performance, and the reaction mechanism need to be carefully considered.

In this paper, alkali metal oxides supported on SBA-15 catalysts, M/SBA-15 (M = Li, Na, K, Rb, and Cs), were prepared by the impregnation method in order to obtain catalysts with different base properties. The interaction of the alkali metals with support, the properties of the basic sites and their influence on the catalytic performance were studied with both experimental and quantum chemical calculations. It was found that the supported alkali metals react with hydroxyl groups on SBA-15 by replacing the H atoms. On M/SBA-15 two types of basic sites (i.e., weak and medium) can be distinguished. With increasing basicity of the alkali metal oxides, the strength and density of the medium basic sites increase. The medium basic sites play an important role in promoting the reaction. On the basis of the quantum calculation results, a pathway with the adsorbed enol molecule as an intermediate was suggested to be predominant for the formation of MA.

2. EXPERIMENTAL SECTION

2.1. Catalyst Preparation. The catalysts were prepared by the impregnation method. Certain amount of alkali metal nitrate was dissolved in deionized water to form salt solution; then SBA-15 (purchased from Shanghai ZZBIO CO., LTD) was impregnated by the solution. After aging for 4 h, excessive water was evaporated at 393 K overnight under atmospheric pressure. Subsequently, the solid was calcined at 823 K for 5 h. The amount of each alkali metal loaded is ca. 0.37 mmol/g.

2.2. Characterization. The surface morphologies of the catalyst samples were checked using a transmission electron microscope (JEM-2010, JEOL) with an acceleration voltage of 200 kV. Meanwhile energy dispersive spectroscopy (EDS) mappings were also performed for the selected areas.

X-ray diffraction (XRD) patterns were collected on an X-ray diffractometer (D/max 2500 VB2, Rigaku) using Cu Kα radiation (λ = 0.15406 nm). Data were recorded in the 2θ range of 0.5°−5° for small-angel XRD and 10°−90° for wide-angle XRD.

The BET specific surface areas were determined from nitrogen adsorption isotherm at liquid nitrogen temperature using an accelerated surface area and porosimetry system (ASAP 2420, Micrometrics). Specific surface areas were calculated using the BET model, and pore size distributions were evaluated from the desorption branches of nitrogen isotherms using the BJH model. Before measurement, the samples were degassed at 573 K for 3 h.

The alkali metal content of the catalysts was determined by ICP-MS (Agilent 7700 series). Alkali metal content of each sample was measured six times. The relative standard deviation for alkali metal content of each sample is in the range of 5%.

Acid−base properties of the catalysts were measured with temperature-programmed desorption (TPD) of CO_2 and NH_3 on an AutoChem II 2920. In a standard procedure, 80 mg sample was activated in a He stream (20 mL min^{-1}) at 823 K for 2 h. Then a stream containing 10 vol % CO_2 or NH_3 passed through the sample during 30 min. After that, the sample was heated in a He stream (20 mL min^{-1}) with a heating rate of 10 K min^{-1} up to 823 K. The desorbed species were analyzed using an online thermal conductivity detector (TCD). On the basis of the ICP-MS measured alkali metal contents and CO_2-TPD results, the moles of CO_2 adsorbed per mole of alkali metal (q) were estimated.

X-ray photoelectron spectroscopy (XPS) spectra were recorded on a photoelectron spectrometer (ESCALAB 250, Thermo Fisher Scientific) using Al Kα excitation at pass energies of 200 eV for survey and 30 eV for high-resolution scans. The binding energy (BE) was calibrated with respect to the C 1s value of a contaminated carbon at 284.9 eV (estimated error ± 0.05 eV).

DOI: 10.1021/acs.iecr.7b02841
Ind. Eng. Chem. Res. 2018, 57, 2773−2786

Fourier transform infrared spectroscopy (FTIR) spectra were recorded on a Thermo Nicolet 8700 spectrometer in the range of 400−4000 cm^{-1}.

In order to determine the nature of the coke on the deactivated catalysts, the used Cs/SBA-15 was immersed in CH_2Cl_2 and treated by ultrasonic wave for 4 h. The obtained solution was analyzed using GC/MS (GC-2010, Shimadzu) equipped with Rtx-5 capillary column.

CP/MAS ^{13}C NMR measurement of used Cs/SBA-15 was carried out using 600 MHz NMR spectrometer (JNM-ECZ600R, JEOL RESONANCE Inc.). The cross−polarization contact time is 2 ms, and the cycle time is 3 s.

Thermogravimetric analysis of the used Cs/SBA-15 was performed on TGA/DSC 1/1100SF analyzer (Mettler Toledo) under an air flow of 50 mL min^{-1} from 313 K up to 1073 K with heating rate of 10 K min^{-1}.

2.3. Catalyst Test. A continuous flow fixed bed tubular reactor made of stainless steel was used to evaluate the catalytic performance under atmospheric pressure. The inner diameter of the tube is 14 mm, and the length is 645 mm. A thermocouple well with an outer diameter of 6 mm is inserted in tube. Before the evaluation, the catalyst powder was pressed, crushed, and sieved to 20−40 mesh. In every test, 2.0 mL catalyst was packed in the middle of the reactor, the upper and lower sections of the catalyst bed were sealed using quartz sand. The reactor was heated by an electric furnace containing two heating blocks.

In this study, trioxymethylene was used instead of FA since pure FA is not easily obtained and difficult to handle. At elevated temperature, trioxymethylene can be easily decomposed to FA stoichiometrically.[26] This has been verified by the gas chromatograph analysis. Though formalin, an aqueous solution containing about 37% of FA, is commercially available, it is usually not used as the feedstock since the water contained shows a hindering effect on aldol condensation reactions.

In the experiments, a solution containing of Ma, trioxymethylene, and methanol was pumped into the upper section of reactor. Methanol helped dissolve trioxymethylene and suppress the decomposition of Ma and MA during the reaction. After the reaction, the products were cooled with a circulated coolant of 268 K and introduced into a gas−liquid separator. The liquid products were analyzed using a gas chromatograph equipped with a flame ionization detector (FID) and a KB-WAX capillary column (0.25 mm × 30 m × 0.25 μm). The products were quantified using the internal standard method with 1-propanol as the internal standard substance. Considering the quantification of FA was not accurate enough due to the very low response of FA on FID, only the molar balance of Ma was calculated supposing that the reaction products of Ma are MA, Aa, and acrylic acid (AA). The calculated molar balance of Ma was in the range of 98.0%−99.9% (see Table S2), indicating that the quantification of the reaction products is reliable.

Conversion of Ma (X), selectivity of i component (S_i), and yield of i component (Y_i) are defined as follows:

$$X(\%) = \frac{n_0 - n_t}{n_0} \times 100 \tag{1}$$

$$S_i(\%) = \frac{n_i}{n_0 - n_t} \times 100 \tag{2}$$

$$Y_i(\%) = \frac{n_i}{n_0} \times 100 \tag{3}$$

where n_0 is the molar flow of Ma fed into the reactor and n_t and n_i are the molar flow of Ma and the i component flowing out of the reactor, respectively.

2.4. Regeneration of Deactivated Catalysts. After reaction, the catalyst was cooled down from reaction temperature to 473 K under a nitrogen flow of 100 mL min^{-1}. Then the nitrogen was switched to air (100 mL min^{-1}), and the temperature of the reactor was increased from 473 to 823 K with a step of 50 K and maintained at each step for 30 min. Finally, the catalyst was calcined at 823 K for 5 h.

2.5. Computational Methods. For the quantum calculations, a Si_{12} cluster consisting of a 5- and a 6-member ring was used as the model of SBA-15.[27] The cluster contains three hydroxyl groups, and one of them was replaced by an alkali metal atom. Geometric optimization and energy calculation were performed in Gaussian 09 program.[28] Wave function analysis was carried out using Multiwfn 3.3 program;[29] unless otherwise specified the default settings of the program were used. The color mapped isosurface graphs of electrostatic potential (ESP) and average local ionization energy (ALIE) were rendered by VMD 1.9 program.[30] The B3LYP[31] hybrid density function, combined with 6-31G(d) basis set, was employed for H, O, Si, Li, Na, and K, and the Lanl2dz pseudopotential basis set was employed for Rb and Cs to optimize the geometries of the reactants and products and to search the transition states. The single point energy for the model involving H, O, Si, Li, Na, and K was calculated at the B3LYP/6-311+G(2d,p) level, and for the model involving Rb and Cs, it was calculated at the B3LYP/Lanl08 level. All of the energies obtained from the DFT calculations used for energy barriers were corrected for the zero-point energy. The dangling bonds of Si in the cluster were saturated using H atoms, and their positions were fixed in order to keep the framework of SBA-15 stable.

3. RESULTS AND DISCUSSIONS

3.1. Experimental Part. *3.1.1. Characterization Results.* The TEM images of SBA-15 and M/SBA-15 are presented in Figure 1. Well-ordered channels are observed for SBA-15, and the uniformity of the texture is reserved after impregnation of alkali metal oxides. The EDS mapping image of Cs/SBA-15 is shown in Figure 2, and those of other catalyst samples (Na/SBA-15, K/SBA-15, and Rb/SBA-15) are shown in Figures S1−S3. It can be seen that the alkali metal oxides are uniformly distributed on the SBA-15 support.

The small-angle XRD patterns of SBA-15 and M/SBA-15 are presented in Figure 3. After supporting Li, Na, and K, the small-angle XRD patterns of the catalysts are essentially the same as that of SBA-15. For Rb and Cs, however, the small-angle XRD patterns show some changes. The diffraction peak at ca. 0.93° of 2θ, referring to planes (1 0 0), shifts to a higher degree and becomes sharper and higher. In addition, the diffraction peaks at 1.61° and 1.89° of 2θ, referring to planes (1 1 0) and (2 0 0), become visible. These changes indicate that upon the supporting of Rb and Cs and calcining at 823 K, the mesoporous framework of these two samples shrunk due to silicon framework condensation. This phenomenon is consistent with the observation for metal oxide supported on SBA-15 catalysts.[32−34]

The wide-angel XRD patterns of SBA-15 and M/SBA-15 are shown in Figure S4. Only a broad diffraction peak at ca. 25° of 2θ ascribed to the amorphous silica appears. In addition, no diffraction peak belonging to the crystalline phase of the alkali

DOI: 10.1021/acs.iecr.7b02841
Ind. Eng. Chem. Res. 2018, 57, 2773−2786

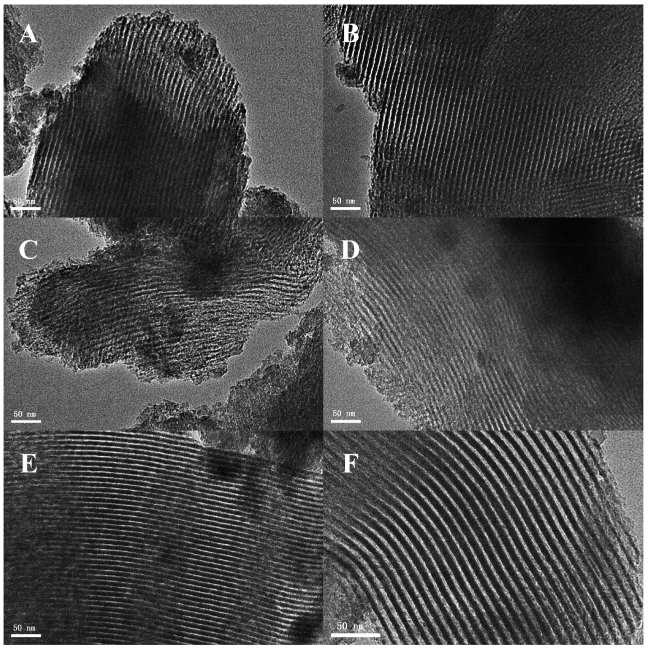

Figure 1. TEM images of (A) SBA-15, (B) Li/SBA-15, (C) Na/SBA-15, (D) K/SBA-15, (E) Rb/SBA-15, and (F) Cs/SBA-15 taken from the direction vertical to the channel axis.

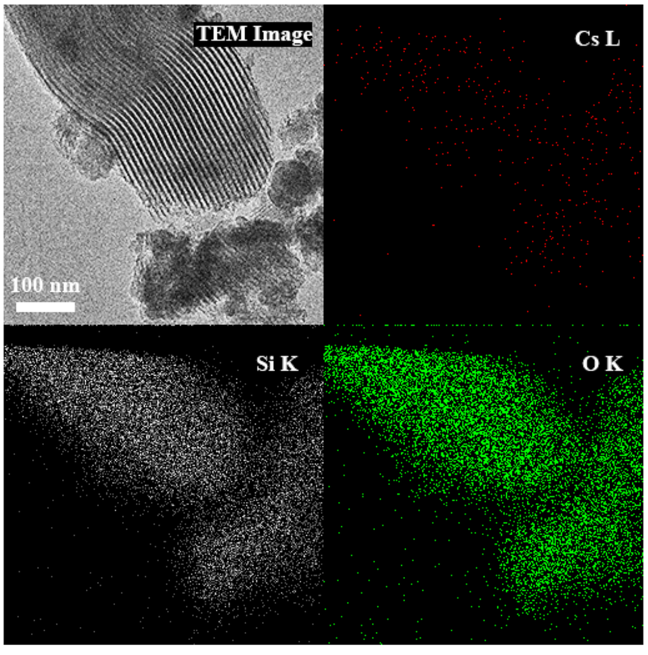

Figure 2. TEM and EDS mapping images of the Cs/SBA-15 catalyst.

metal oxide presents in the XRD patterns of M/SBA-15, which means that the alkali metal oxides are well-dispersed on these catalysts.[32]

The textural properties of SBA-15 and M/SBA-15 are listed in Table 1. N_2 adsorption−desorption isotherm and pore size distribution of SBA-15 and M/SBA-15 are presented in Figures S5−S10. The SBA-15 support has a specific BET surface area of 493 m^2/g, a pore volume of 0.53 cm^3/g, and an average pore diameter of 4.6 nm. Upon supporting the alkali metal oxides, the BET specific area and the pore volume of the samples decrease noticeably. The extent of the decrease depends on the nature of the supported metal, with Na/SBA-15 and K/SBA-15

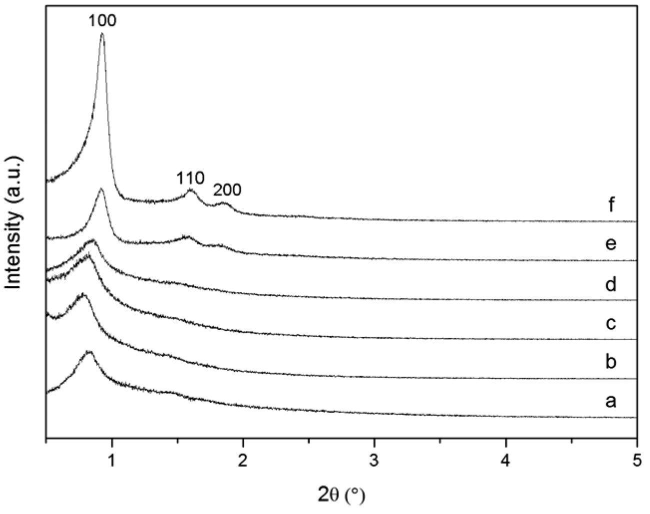

Figure 3. Small-angle XRD patterns: (a) SBA-15, (b) Li/SBA-15, (c) Na/SBA-15, (d) K/SBA-15, (e) Rb/SBA-15, and (f) Cs/SBA-15.

giving more significant reduction. The reduced BET specific surface area of the M/SBA-15 indicates that sintering of the amorphous silica occurs upon supporting the alkali metals and subsequently calcining at 823 K.

The contents of the alkali metal in the catalysts were measured by ICP-MS and listed in Table 1. It can be seen that the measured alkali metal contents (with a maximum deviation of 0.02 mmol/g) are very close to that added in the preparation of the catalysts.

CO_2-TPD profiles of the M/SBA-15 catalysts are presented in Figure 4. In accordance with the modes of CO_2 adsorption on different basic sites, each basic site adsorbs one CO_2 molecule. So the densities of basic sites on the M/SBA-15 can be estimated, which are listed in Table 2. The density of the basic sites on the M/SBA-15 increases from 0.076 mmol/g (Li/SBA-15) to 0.110 mmol/g (Rb/SBA-15). The similar trend has been observed by Díez et al.[23] on Na, K, and Cs/MgO with an alkali metal loading of 1 mol %. Tai et al.[35] measured the density of the basic sites on Cs/SiO_2 with alkali metal loading of 4% in terms of CO_2-TPD, and a value of 0.073 mmol/g was reported. Compared to the previous study, the density of the basic sites measured in this work is quite reasonable.

For each catalyst in this work, deconvolution of the CO_2-TPD desorption peak generates four subpeaks. The desorption temperature of the subpeaks and the corresponding densities of the basic sites are given in Table 2. According to the results of Díez et al.,[23] the basic sites on the M/SBA-15 catalysts of this study can be classified into two groups (i.e., the weak basic sites consisting of peak 1 and peak 2, referred as WB-I and WB-II and the medium basic sites consisting of peak 3 and peak 4, referred as MB-I and MB-II). The temperature of the subpeaks indicates that the strength of the weak basic sites on the M/SBA-15 catalysts is approximately the same, while those of the medium basic sites show significant differences, depending on the basicity of alkali metal oxides. On the Na, K, Rb, and Cs/SBA-15, the strength of the medium basic sites of MB-I (404−407 K) is approximately the same but slightly weaker than that of Li/SBA-15 (419 K). On the K, Rb, and Cs/SBA-15, the strength of the medium basic sites of MB-II (480−481 K) is the same but noticeably stronger than that on Na/SBA-15 (458 K) and Li/SBA-15 (438 K).

DOI: 10.1021/acs.iecr.7b02841
Ind. Eng. Chem. Res. 2018, 57, 2773−2786

Table 1. Textural and Physicochemical Properties of SBA-15 and M/SBA-15

catalysts	S_{BET} (m^2/g)	pore volume (cm^3/g)	average pore diameter (nm)	alkali metal content (mmol/g)[a]	alkali metal content (mmol/g)[b]	q^c	TOF[d] (10^{-3})
SBA-15	493	0.53	4.6	–	–	–	–
Li/SBA-15	269	0.47	5.5	0.37	0.35	0.22	3.16
Na/SBA-15	224	0.39	5.5	0.37	0.35	0.24	4.26
K/SBA-15	200	0.37	5.9	0.37	0.38	0.25	8.89
Rb/SBA-15	247	0.46	6.0	0.36	0.37	0.30	9.07
Cs/SBA-15	266	0.48	6.0	0.36	0.35	0.29	10.52

[a]The data was calculated theoretically. [b]The data was analyzed by ICP-MS. [c]Moles of CO_2 adsorbed/mol alkali metal analyzed by ICP-MS. [d]Moles of Ma conversion/mol of basic site/s.

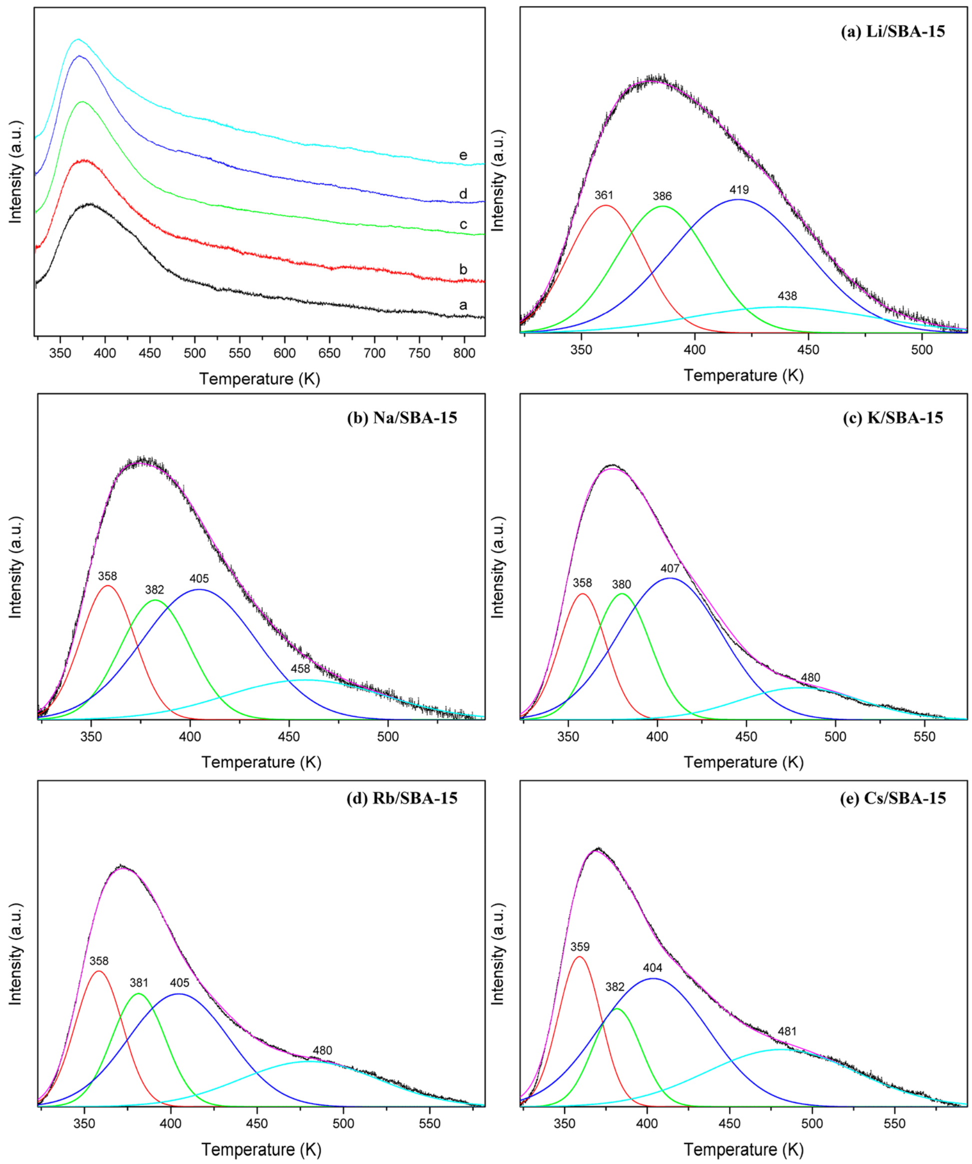

Figure 4. CO_2-TPD profile of (a) Li/SBA-15, (b) Na/SBA-15, (c) K/SBA-15, (d) Rb/SBA-15, and (e) Cs/SBA-15 catalysts.

Concerning the distribution of the basic sites with different strength, Rb/SBA-15 shows the highest density of the weak basic sites (0.045 mmol/g), followed by K/SBA-15 (0.038 mmol/g) and Li, Na, and Cs/SBA-15 (about 0.035 mmol/g). The densities of the medium basic sites increase with increasing basicity of the alkali metal oxides from Li/SBA-15 (0.039 mmol/g) to Cs/SBA-15 (0.069 mmol/g).

For the aldol condensation reaction, some research has mentioned that the acidic sites play important roles in the activation of FA. For instance, Gogate et al.[36] Zhang et al.,[18] and Tai et al.[35] used V–Si–P, Cs–P/γ-Al_2O_3, and Cs/SiO_2, Cs/γ-Al_2O_3, and Cs/ZrO_2 as the catalysts for the aldol condensation reactions. On these catalysts, there are strong acidic sites either produced by doping with P or coming from the supports such as γ-Al_2O_3 and ZrO_2. The acidic properties of

DOI: 10.1021/acs.iecr.7b02841
Ind. Eng. Chem. Res. 2018, 57, 2773–2786

Table 2. CO_2-TPD Results of M/SBA-15

catalysts	density of basic sites (mmol/g)	desorption peak center (K)				distribution of density of basic sites (mmol/g)			
		peak 1	peak 2	peak 3	peak 4	peak 1	peak 2	peak 3	peak 4
Li/SBA-15	0.076	361	386	419	438	0.016	0.020	0.031	0.008
Na/SBA-15	0.083	358	382	405	458	0.016	0.019	0.034	0.014
K/SBA-15	0.094	358	380	407	480	0.017	0.021	0.044	0.012
Rb/SBA-15	0.110	358	381	405	480	0.023	0.022	0.041	0.023
Cs/SBA-15	0.103	359	382	404	481	0.020	0.014	0.043	0.026

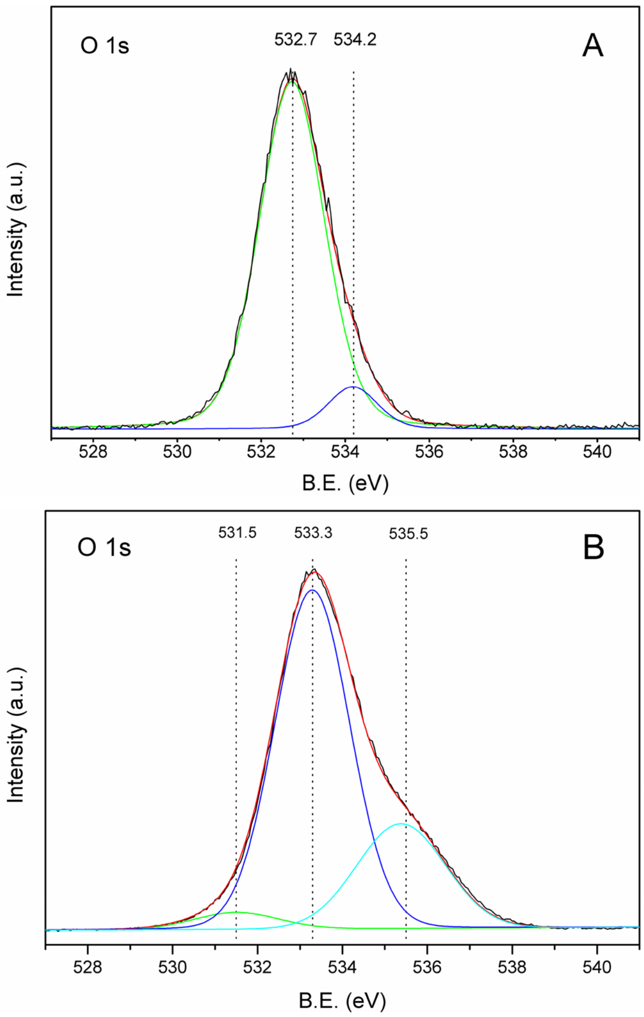

Figure 5. X-ray photoelectron spectra for the O 1s region of (A) SBA-15 and (B) Cs/SBA-15.

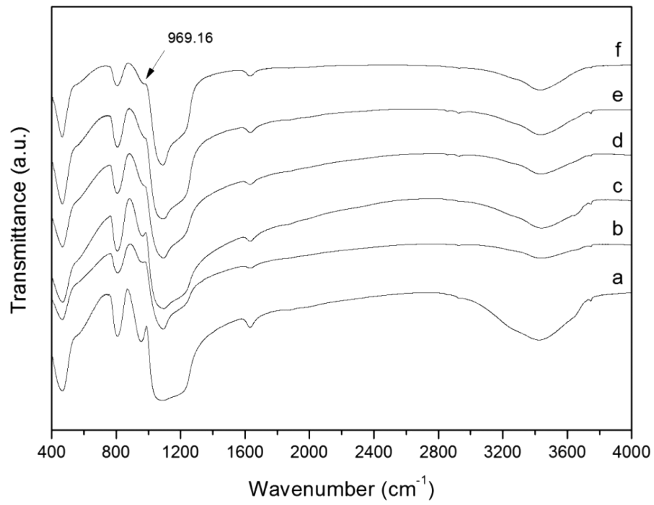

Figure 6. FTIR results of (a) SBA-15, (b) Li/SBA-15, (c) Na/SBA-15, (d) K/SBA-15, (e) Rb/SBA-15, and (f) Cs/SBA-15.

SBA-15 and M/SBA-15 catalysts were investigated using the NH_3-TPD, which is shown in Figure S11. The densities of acidic sites on these catalysts are given in Table S1. The low desorption temperature of NH_3 (around 373 K) and the high density suggest that the acidic sites are most likely to be Si−OH groups on the SBA-15 support.[37] The strength of the acidic sites on M/SBA-15 seems too weak[38] to activate FA, and their role in the aldol condensation reaction of Ma and FA is not considered in this study.

The XPS results of SBA-15 are shown in Figure 5A. One peak at about 533 eV belonging to the oxygen species was observed. Deconvolution of this peak gives two subpeaks at 532.7 and 534.2 eV. The former can be attributed to the oxygen species connected to silicon (Si−O, 532.7 eV) while the latter to the oxygen species connected to hydrogen in OH or H_2O (534.2 eV).[39]

The XPS results of Cs/SBA-15 are shown in Figure 5B and Figure S12. The peaks at 726.0 and 739.9 eV shown in Figure S12 can be attributed to Cs $3d_{5/2}$ and Cs $3d_{3/2}$.[40−42] Figure 5B shows that deconvolution of the peak at 533 eV gives three subpeaks at 531.5, 533.3, and 535.5 eV, respectively. The peak at 531.5 eV is attributed to the oxygen species connected to Cs.[42] The peak at 533.3 eV is attributed to the oxygen species connected to Si.[39] The peak at 535.5 eV is attributed to the oxygen species of hydroxyl groups.[39] The XPS results of Cs/SBA-15 indicate that after impregnation of cesium, the H atoms of the surface hydroxyl groups can be replaced by cesium. However, this replacement is not complete; there is still some hydroxyl groups left on the catalyst surface. This can also be verified by the results of FTIR shown in Figure 6.

Figure 6 gives the FTIR spectra of SBA-15 and M/SBA-15. The peaks at 470, 800, 1070, 1220 cm^{-1} are the characteristic vibration of condensed Si−O−Si.[43] The peak at about 960 cm^{-1} is the characteristic absorption of noncondensed Si−OH.[43] Upon the impregnation of alkali metal oxide, this peak becomes weak, indicating that the alkali metal oxides can react with the silanol groups,[11,44] resulting in the replacement of the H atom of Si−OH by alkali metals. The peak around 1630 cm^{-1} is due to the bending vibration of H_2O, which adsorbs on the catalysts.[43]

3.1.2. Catalytic Performance. The catalytic performance of SBA-15 and M/SBA-15 in the vapor phase aldol condensation of Ma and FA was evaluated under the following conditions: T = 663 K; liquid hourly space velocity (LHSV) = 1.8 h^{-1}; Ma:FA:methanol = 1:2:2 (molar ratio). The selection of the reaction conditions was based on references,[12,18,45,46] in which

DOI: 10.1021/acs.iecr.7b02841
Ind. Eng. Chem. Res. 2018, 57, 2773−2786

Table 3. Catalytic Activity of SBA-15 and M/SBA-15 at Different Time on Stream

catalysts	conversion of Ma (%)/yield of MA (%) 1 h	2 h	3 h	4 h
SBA-15	0.84/0.74	0.51/0.42	0.80/0.43	1.07/0.57
Li/SBA-15	5.14/3.11	5.05/3.18	3.87/2.86	3.96/3.11
Na/SBA-15	7.61/7.13	6.92/6.54	6.13/5.90	5.87/5.44
K/SBA-15	17.89/17.32	16.74/16.48	15.80/15.60	14.55/14.37
Rb/SBA-15	21.31/20.82	19.45/18.57	18.14/17.65	16.38/15.73
Cs/SBA-15	23.20/22.81	20.75/20.51	18.62/18.35	16.33/15.86

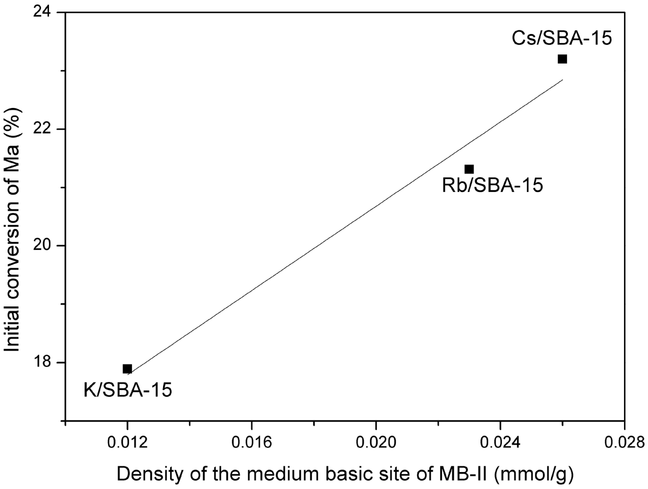

Figure 7. Initial conversion of Ma as a function of density of MB-II on M/SBA-15 (M = K, Rb, and Cs). Reaction conditions: temperature = 663 K, LHSV = 1.8 h^{-1}, and molar ratio of Ma:FA:methanol = 1:2:2.

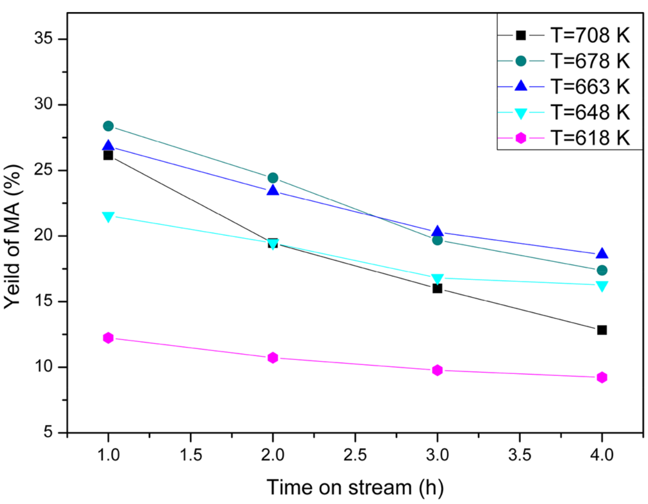

Figure 8. Effect of temperature on the MA yield over Cs/SBA-15. Reaction conditions: LHSV = 1.8 h^{-1} and molar ratio of Ma:FA:methanol = 1:2:2.

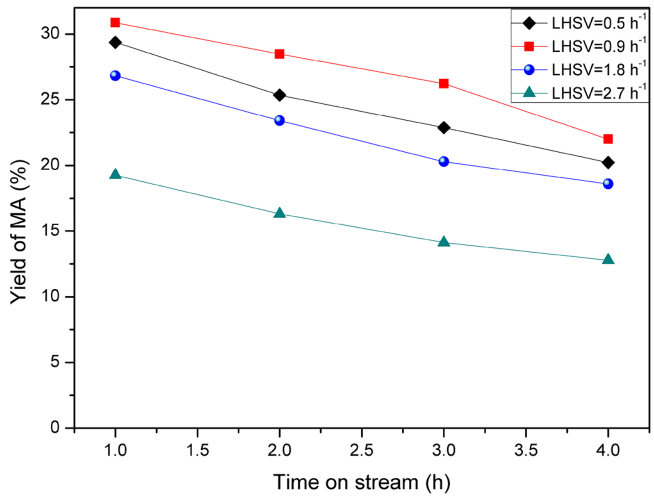

Figure 9. Effect of LHSV on the MA yield over Cs/SBA-15. Reaction conditions: temperature = 663 K and molar ratio of Ma:FA:methanol = 1:2:2.

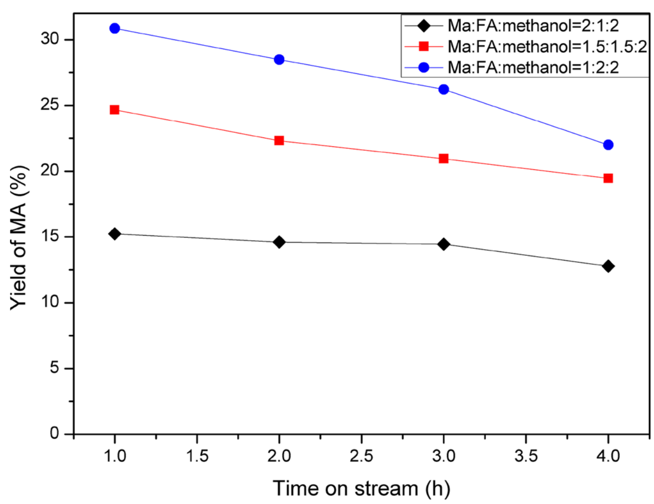

Figure 10. Effect of the molar ratio of Ma to FA on the MA yield over Cs/SBA-15. Reaction conditions: temperature = 663 K and LHSV = 0.9 h^{-1}.

Cs/SBA-15, Cs–P/γ-Al_2O_3, V–P oxides, and Ba/Al_2O_3 were used as catalysts, and the reaction was usually conducted at T = 643–663 K and LHSV = 1.2–1.8 h^{-1}.

The conversion of Ma and yield of MA are presented in Table 3. On SBA-15, the conversion of Ma and the yield of MA are both less than 1%. On M/SBA-15, an increase in both the conversion of Ma and the yield of MA is observed. With increase in the basicity of the alkali metal oxides from Li to Cs, the conversion of Ma and the yield of MA follow the sequence: Cs > Rb > K > Na > Li.

From the data of Table 3, it can be seen that the activity sequence of M/SBA-15 catalysts is consistent with the sequence of the strength and density of the medium basic sites, especially those of MB-II. As indicated by the CO_2-TPD (Table 2 and Figure 4), the strength of the basic sites of MB-II on K, Rb, and Cs/SBA-15 is the same but obviously stronger than that on Li, Na/SBA-15. This results in an abrupt increase of the initial conversion of Ma from 5.14 to 7.61% on Li, Na/SBA-15 to 17.89–23.20% on K, Rb, and Cs/SBA-15. On K, Rb,

DOI: 10.1021/acs.iecr.7b02841
Ind. Eng. Chem. Res. 2018, 57, 2773–2786

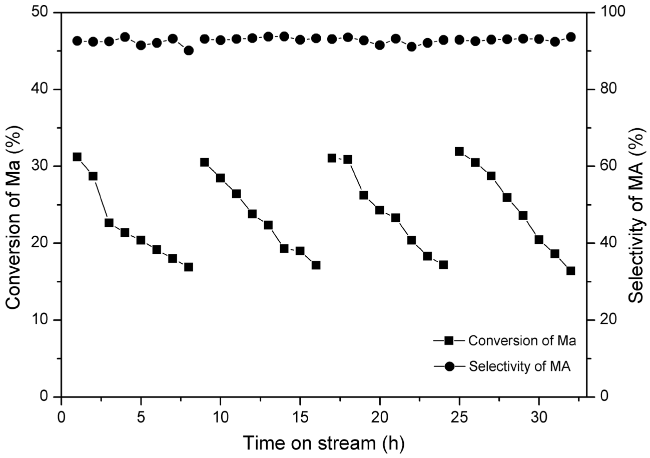

Figure 11. Conversion of Ma and the selectivity of MA over Cs/SBA-15 in three regenerated cycles. Reaction conditions: temperature = 663 K, LHSV = 0.9 h^{-1}, and molar ratio of Ma:FA:methanol = 1:2:2.

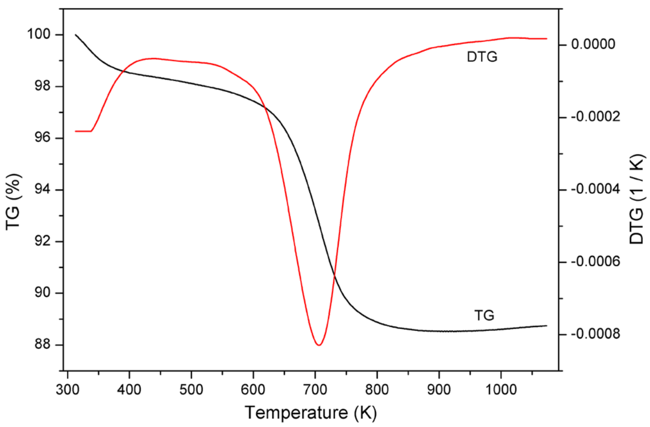

Figure 12. TG-DTG curve of used Cs/SBA-15 catalyst.

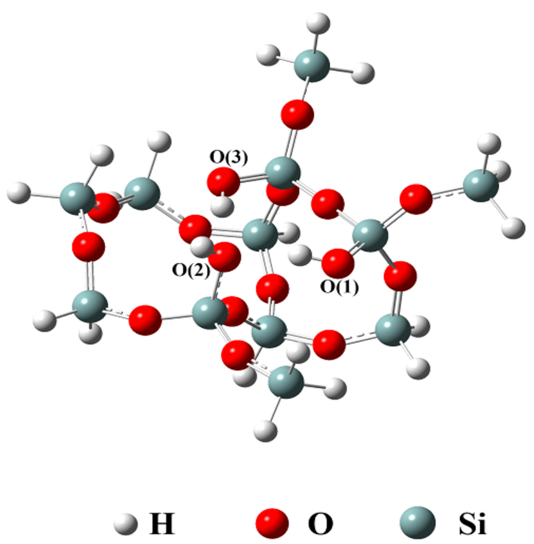

Figure 13. Model of SBA-15.

and Cs/SBA-15, the strength of medium basic sites is the same, while the density of the medium basic sites of MB-II increases in a sequence of K < Rb < Cs. This sequence coincides with the initial conversion of Ma on these catalysts as shown in Figure 7, in which the initial conversion of Ma on K, Rb, and Cs/SBA-15 is linearly correlated with the density of the MB-II basic site. The above-mentioned observations concerning the influence of the strength and density of the basic sites on M/SBA-15 imply that the medium basic site MB-II plays an important role for the aldol condensation of Ma and FA.

The values of q and the turnover frequencies (TOFs) calculated based on the initial conversion of Ma are given in Table 1. With the same alkali metal loading (ca. 0.37 mmol/g), the value of q is ca. 0.30 for Rb and Cs, which is slightly higher than that of Li, Na, and K (0.22–0.25). This means that the amount of surface basic sites generated by alkali metal oxides and the extent of the aggregation of the alkali metal oxides are similar.[24] The TOFs of M/SBA-15 catalysts monotonously increase from Li to Cs. From the comparison of the q and TOFs, the different activities observed for different alkali metal oxides can be mainly ascribed to the different basicity of the metals.

With increasing time on stream, the conversion of Ma as well as the yield of MA decreases on all of the catalysts, which can be attributed to the deactivation of the catalysts due to coke deposition as evidenced by the black color in the presence of the coke on the catalysts.

The catalyst test results shown in Table 3 indicate that Cs/SBA-15 has the highest initial conversion of Ma (23.20%) and the highest initial yield of MA (22.81%). To investigate the effect of the reaction conditions on the catalyst performance, tests at different temperatures, LHSVs, and molar ratios of the reactants have been carried out on Cs/SBA-15 catalyst.

Figure 8 presents the results obtained at temperatures from 618 to 708 K. With increasing temperature from 618 to 678 K, the initial yield of MA increases. However, the higher temperature at 708 K leads to a lower initial yield of MA. The catalyst shows an approximately equal deactivation rate in the temperature range from 618 to 663 K. At temperature higher than 663 K, the catalyst shows a faster deactivation rate, indicating that coke deposition and side reaction are significantly accelerated at higher temperature.

Figure 9 presents the influence of LHSV on the yield of MA at 663 K with a molar ratio of Ma:FA:methanol = 1:2:2. The LHSV varied from 0.5 to 2.7 h^{-1}. A maximum yield of MA is observed at 0.9 h^{-1}. The approximately same slope of the yield versus time curves implies that the catalyst deactivates at an approximately same rate at different LHSVs. The lower yield of MA at LHSV of 0.5 h^{-1} is due to the lower selectivity of MA, indicating that longer contact time leads to further conversion of Ma to other side products. While the lower yield of MA observed at higher LHSV is due to the lower conversion of Ma.

Figure 10 shows the results obtained at molar ratio of FA to Ma from 0.5 to 2 mol/mol at 663 K and LHSV of 0.9 h^{-1}. As can be seen from this figure, increasing the molar ratio of FA to Ma will increase the conversion of Ma and consequently the yield of MA.

In this study, the highest yield of MA is ca. 31% which is obtained at 663 K with a LHSV of 0.9 h^{-1} and a molar ratio of Ma:FA:methanol being 1:2:2. The same reaction has been studied by Yan et al.[12] over a Cs/SBA-15 catalyst, and a yield of MA of ca. 46% was obtained at 663 K with a molar ratio of Ma:FA being 1:2. The lower yield of the MA in this study could have resulted from the dilution effect of methanol in the feed. Bao et al.[46] reported a MA yield of ca. 26%, obtained over a Cs/Al_2O_3 catalyst at 663 K and a molar ratio of Ma:FA:methanol being 1:2:2. Therefore, the performance of the catalysts of this study is comparable with the previous reports.

DOI: 10.1021/acs.iecr.7b02841
Ind. Eng. Chem. Res. 2018, 57, 2773–2786

Table 4. Energies of M/SBA-15 (Hartree)

	Li/SBA-15	Na/SBA-15	K/SB-15	Rb/SBA-15	Cs/SBA-15
energy of M-O(1)/SBA-15	−4699.84	−4854.60	−5292.25	−4716.17	−4712.19
energy of M-O(2)/SBA-15	−4699.85	−4854.62	−5292.27	−4716.19	−4712.21
energy of M-O(3)/SBA-15	−4699.84	−4854.59	−5292.25	−4716.17	−4712.19

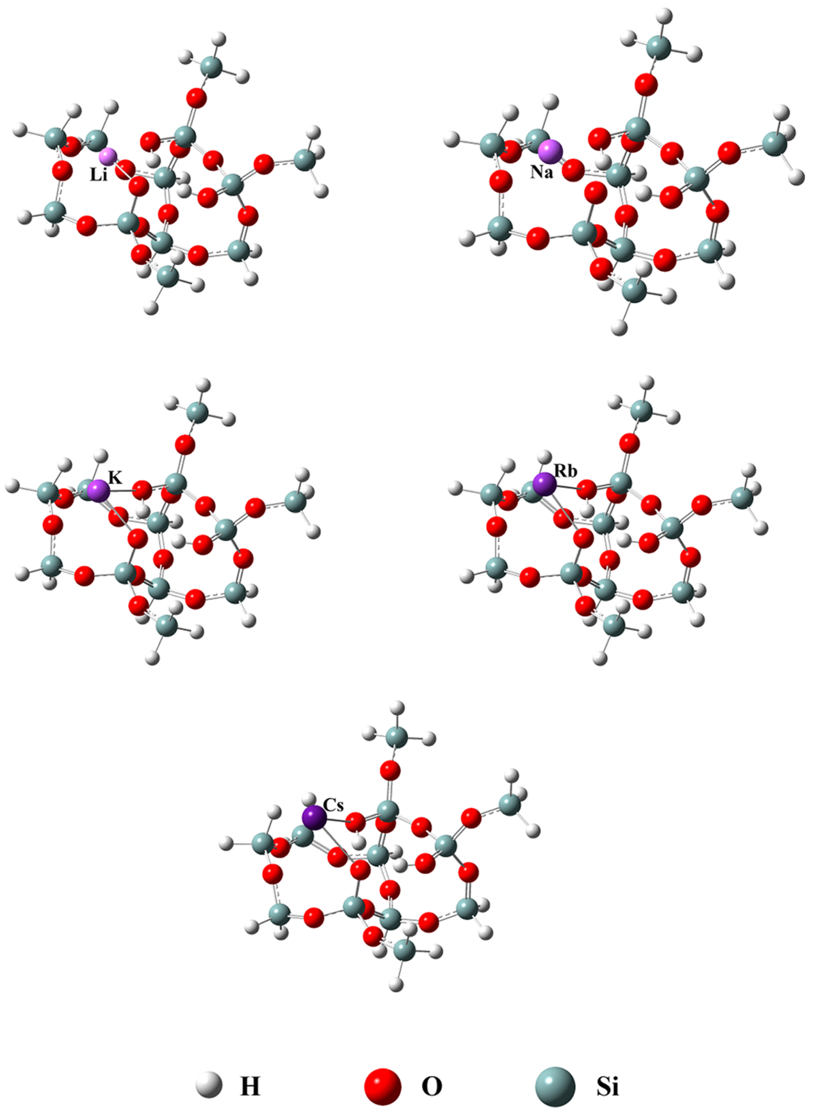

Figure 14. Geometries of M-O(2)/SBA-15.

3.1.3. Catalyst Stability and Reusability. Results concerning the stability and reusability of the Cs/SBA-15 catalyst are shown in Figure 11. The tests were carried out at 663 K with a LHSV of 0.9 h^{-1} and a molar ratio of Ma:FA:methanol being 1:2:2. After 8 h on stream, the conversion of Ma decreases from ca. 30% to ca. 15%. In the three regenerated cycles, the regenerated catalyst shows the same performance as the fresh catalyst. This means that the deactivation of the catalyst is mainly due to coke deposition, and regeneration by burning off the coke can restore the activity of the catalyst.

The thermogravimetric analysis of deactivated Cs/SBA-15 catalyst is shown in Figure 12. TG curve shows two weight loss steps. From 323 K to about 513 K, the physically adsorbed water and small molecules are lost. From 513 K to about 833 K, the weight loss is mainly due to the combustion of deposited coke material.[47] The weight losses of these two stages are 1.87% and 9.53%.

The GC/MS analysis of the CH_2Cl_2 soluble coke formed on Cs/SBA-15 catalyst is shown in Figure S13. The main component is toluene. In addition, small amounts of methylcyclohexane, dimethylcyclohexane, and xylene are also detected. However, GC/MS analysis did not detect the presence of these components in the reaction products, implying that the amount of the above-mentioned compounds is very small. The CP/MAS ^{13}C NMR spectrum of deactivated Cs/SBA-15 catalyst is shown in Figure S14. As can be seen from this figure, the coke consists of aliphatic carbons (0−90 ppm), aromatic carbons (90−160 ppm), and carbonyl carbons (160−220 ppm).[48]

3.2. Computational Part. *3.2.1. Location of Alkali Metal Atoms.* In this work, the structure of SBA-15 is modeled with a

DOI: 10.1021/acs.iecr.7b02841
Ind. Eng. Chem. Res. 2018, 57, 2773−2786

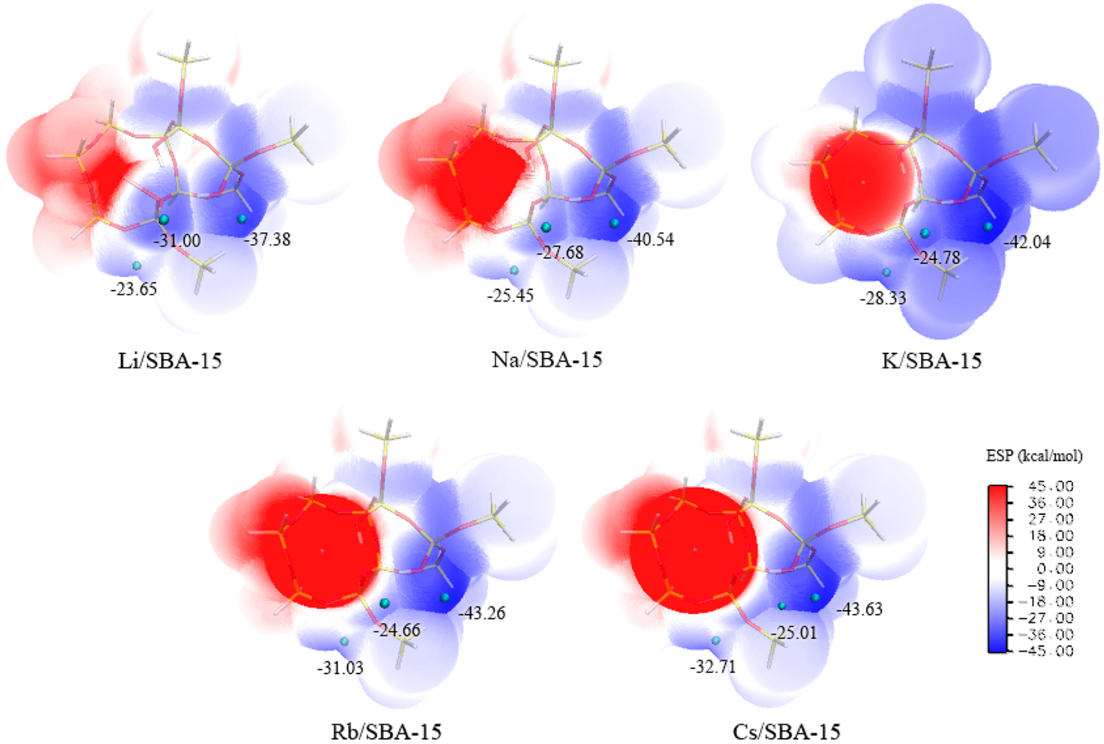

Figure 15. ESP on vdW surface of M/SBA-15.

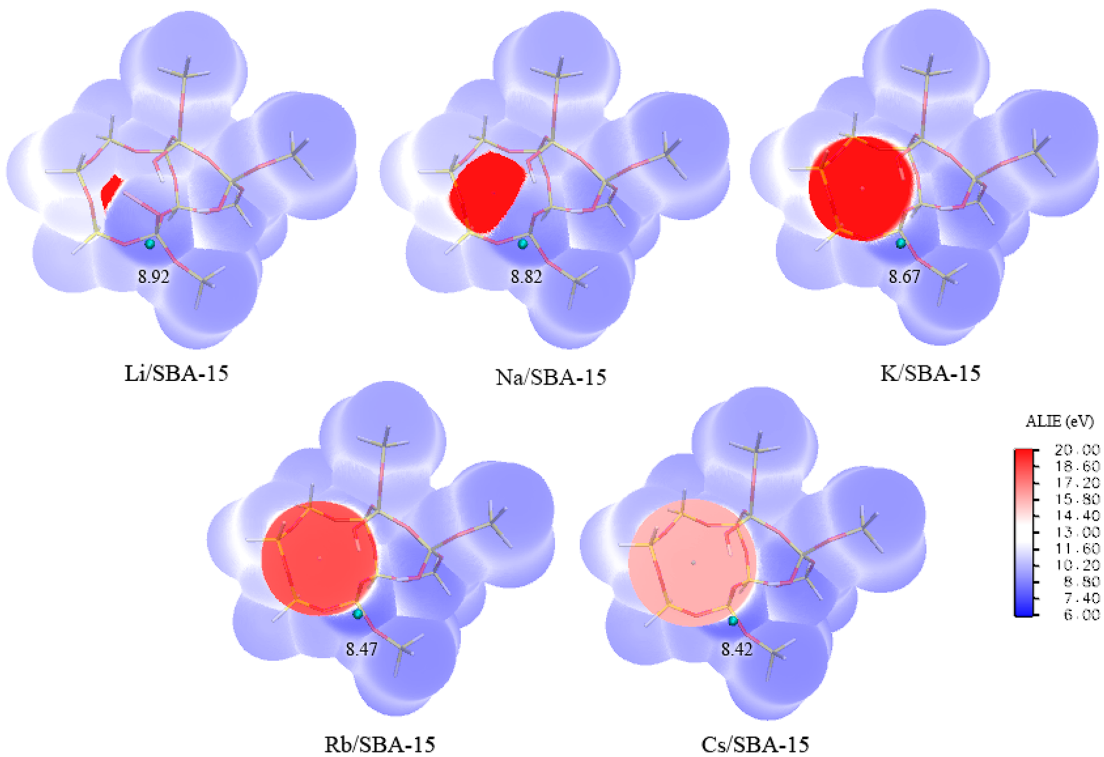

Figure 16. ALIE on vdW surface of M/SBA-15.

method reported by Liu et al.[49] and is shown in Figure 13. This Si_{12} cluster contains a 5- and a 6-member ring, and two Si atoms are shared by these two rings. H atoms were used to saturate the dangling bonds of Si atoms. The location of the terminal H atoms was fixed when optimizing the geometries of M/SBA-15. In this model, three types of surface hydroxyl groups can be distinguished [i.e. H−O(1)/SBA-15, H−O(2)/SBA-15, and H−O(3)/SBA-15]. When the alkali metal atoms substitute the H atoms of silanol groups, they can form three types of M-O species: M-O(1)/SBA-15, M-O(2)/SBA-15, and M-O(3)/SBA-15. The energies of M/SBA-15 under the optimized geometries are given in Table 4. The bond length of M-O(2) and bond angle of Si−O(2)-M are given in Table S3.

DOI: 10.1021/acs.iecr.7b02841
Ind. Eng. Chem. Res. 2018, 57, 2773−2786

Scheme 2. First Pathway of Aldol Condensation of Ma and FA

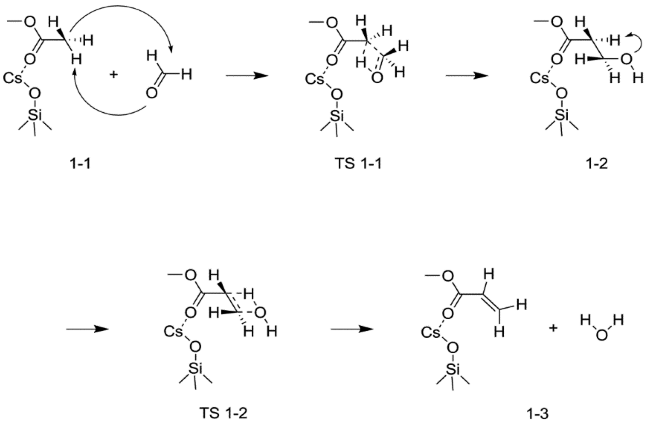

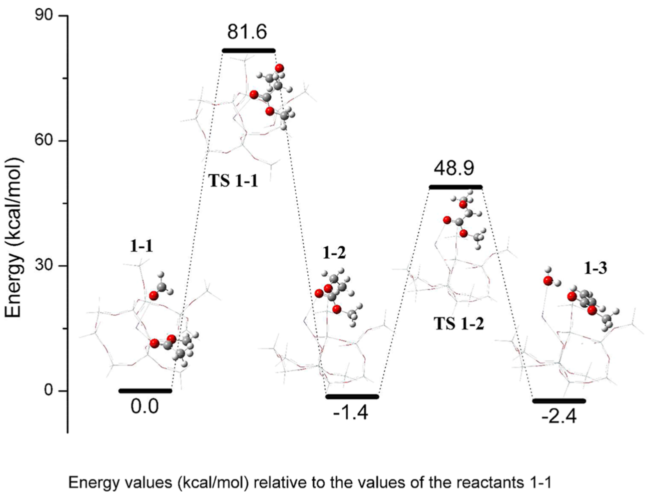

Figure 17. Energy profile for Scheme 2.

As can be seen from Table 4, M-O(2)/SBA-15 has the lowest energy for all of the five alkali metal atoms, which means that the alkali metals prefer reacting with the silanol group of H−O(2)/SBA-15, forming M-O(2)/SBA-15. The geometries of M/SBA-15 are shown in Figure 14.

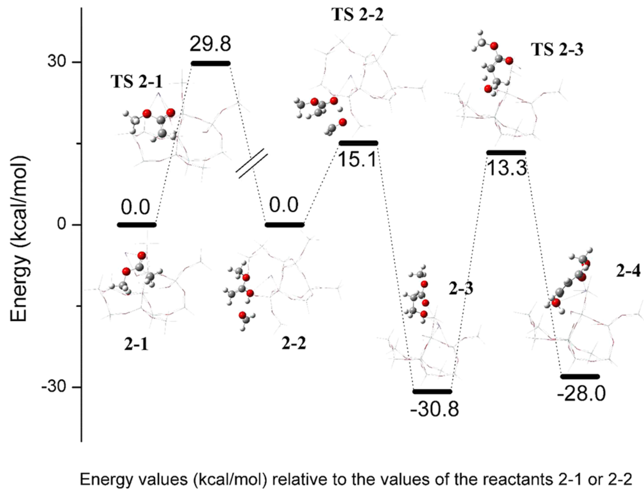

Figure 18. Energy profile for Scheme 3. Two parallel bars indicate that the energy of FA starts to be included, and the following energy values are relative to the reactants 2−2.

3.2.2. Quantitative Analysis of Molecular Surface. ESP and ALIE have been used to predict the active sites of catalysts.[50] A negative value of ESP on van der Waals (vdW) surface means that negative charge is dominant at this site, which has the ability to attract electrophiles.[51] A smaller value of ALIE at point $\boldsymbol{r}$ means a higher electron average energy and a stronger ability for the electron to participate in a chemical reaction. In order to determine the most possible active sites, the distribution of ESP and ALIE on the vdW surface (ρ = 0.001 e/bohr^3) of the catalyst models is calculated.

Figure 15 presents the results of the ESP calculations. Three minima with the lowest values of the ESP are indicated by the cyan points and the values are given in the figure. These minima locate near the O(1) and O(2) atom and are the potential active sites when the electron-deficient part of a molecule approaches them. Since the ESP analysis does not take electron local activity into account, solely using ESP to predict active sites is often not reliable because electrophilic attack involves covalent formation/disruption.[50]

ALIE at a point $\boldsymbol{r}$ can be regarded as an indication of the average energy required to remove an electron at $\boldsymbol{r}$. Figure 16 presents the results of the ALIE calculations. The smallest ALIE

Scheme 3. Second Pathway of Aldol Condensation of Ma and FA

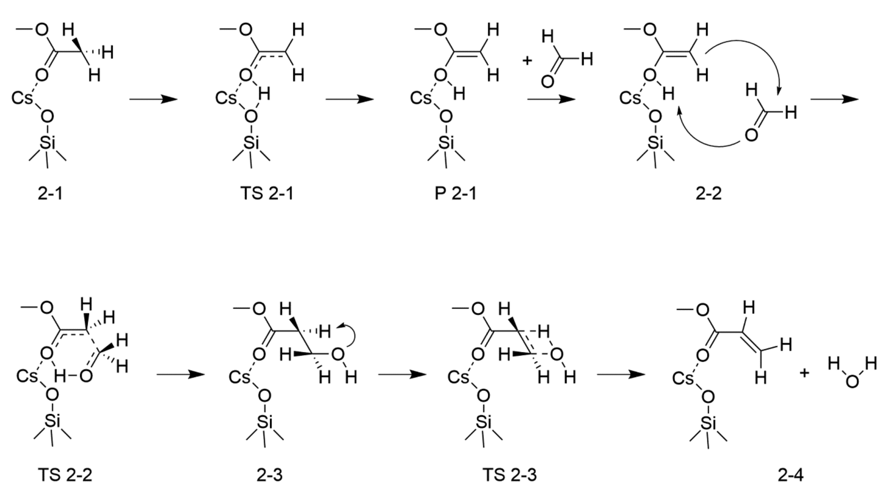

DOI: 10.1021/acs.iecr.7b02841
Ind. Eng. Chem. Res. 2018, 57, 2773−2786

value appears around atom O(2). This indicates that the atom O(2) is the most possible active site for an electron-deficient molecule. It can be noticed that the values of the minima of both ESP and ALIE decrease from Li/SBA-15 to Cs/SBA-15. This means that the catalytic activity of the M/SBA-15 will increase from Li/SBA-15 to Cs/SBA-15, which is in line with the experimental observations in the catalyst tests.

3.2.3. Pathway of Aldol Condensation Reaction. In this study, the two most likely pathways for the vapor phase aldol condensation of Ma and FA on Cs/SBA-15 are investigated using DFT calculations. The first pathway is shown in Scheme 2. Here, we use the Si−O−Cs to represent the active site of Cs/SBA-15 catalyst. In the first pathway, Ma adsorbs on the active site of Cs/SBA-15 by the O atom of the carbonyl group. Then, α-H of Ma was captured by the O atom of the carbonyl group of FA and the α-C of Ma attacks the C atom of FA, forming an intermediate 1−2 via a transition state of TS 1−1. Decomposition of intermediate 1−2 forms the product and releases a H_2O molecule via a transition state of TS 1−2. The energy diagram of the first pathway is given in Figure 17, and the atomic coordinates are given in Tables S4−S8. The energy barrier for the formation of TS 1−1 is 81.6 kcal/mol; for TS 1−2, it is 50.3 kcal/mol.

The second pathway is shown in Scheme 3. First, the O atom of carbonyl group of Ma adsorbs on the Cs atom. Then, the O(2) atom of Cs/SBA-15 captures the α-H of Ma. The captured α-H atom is then transferred to the carbonyl group of Ma via a transition state TS 2−1, forming an adsorbed enol molecule. The adsorbed enol molecule reacts with FA to generate intermediate 2−3 via a transition state of TS 2−2. The intermediate 2−3 decomposes via a transition state TS 2−3, forming the product and releasing a H_2O. The energy diagram of the second pathway is given in Figure 18, and the atomic coordinates are given in Tables S9−S15. The energy barrier for the formation of TS 2−1 is 29.8 kcal/mol; TS 2−2 is 15.1 kcal/mol; and TS 2−3 is 44.1 kcal/mol.

In the first pathway, the rate-determining step is the formation of transition state TS 1−1 with an energy barrier of 81.6 kcal/mol. In the second pathway, the rate-determining step is the decomposition of intermediate 2−3 with an energy barrier of 44.1 kcal/mol. This means that the second pathway is the predominant pathway for the formation of MA on the Cs/SBA-15 catalyst.

4. CONCLUSIONS

Alkali metal oxides supported on SBA-15, M/SBA-15 (M = Li, Na, K, Rb, and Cs) promote the aldol condensation of Ma and FA to MA, while the support is inert. The conversion of Ma and the yield of MA follow the order of the basicity of the alkali metal oxides. On Cs/SBA-15, the highest yield of MA of 31% is obtained at T = 663 K, LHSV = 0.9 h^{-1}, and molar ratio of Ma:FA:methanol = 1:2:2. The supported alkali metals react with hydroxyl groups on the SBA-15 surface by replacing the H atoms. On M/SBA-15, two types of basic sites (i.e., weak and medium) can be distinguished. With increasing basicity of the alkali metal oxides, the strength and density of the medium basic sites increase, which is in line with the experimentally observed performance of the catalysts. This indicates that the medium basic sites play an important role in promoting the reaction.

DFT calculations indicate that the alkali metals prefer reacting with the silanol group of H−O(2)/SBA-15, forming M-O(2)/SBA-15. The analysis of ESP and ALIE indicates that the alkali metal atom and the O(2) atom form the active center on the M/SBA-15 catalysts. The predicated activity of the alkali metal oxides follows the order of their basicity, which is in line with the experimentally observed order of the catalytic activity on these catalysts. Two possible pathways for the formation of MA are proposed. On the basis of the energy barriers of rate-determining steps, the predominant way for the formation of MA is suggested, which involves an adsorbed enol molecule as the reaction intermediate.

The deactivated Cs/SBA-15 catalyst can be regenerated by burning off the coke, and the regenerated catalyst gives practically the same activity as that of the fresh one, indicating that coke deposition is the major factor leading to the deactivation of the catalyst.

■ ASSOCIATED CONTENT

Supporting Information

The Supporting Information is available free of charge on the ACS Publications website at DOI: 10.1021/acs.iecr.7b02841.

TEM and EDS mapping images of M/SBA-15 (M = Na, K, and Rb); wide-angle XRD patterns of SBA-15 and M/SBA-15; N_2 adsorption−desorption isotherm and pore size distribution of SBA-15 and M/SBA-15; NH_3-TPD profiles of SBA-15 and M/SBA-15; X-ray photoelectron spectra for the Cs 3d region of Cs/SBA-15; dissolved composition of coke on the used Cs/SBA-15; cross-polarization ^{13}C NMR spectra of the coke from used Cs/SBA-15; NH_3-TPD results of SBA-15 and M/SBA-15; catalytic activity of SBA-15 and M/SBA-15 and molar balance of Ma; bond length of M-O(2) and bond angle of Si−O(2)-M; and atomic coordinates for reactants, transition states, and products of Scheme 2 and Scheme 3 (PDF)

■ AUTHOR INFORMATION

Corresponding Author

*Address: No. 15 North Third Ring Road, Chaoyang District, Beijing 100029, P. R. China. Tel.: +86 10 6445 4730. Fax: +86 10 6443 6781. E-mail: wangjd@mail.buct.edu.cn.

ORCID

Teng He: 0000-0002-4798-3441
Yixin Qu: 0000-0001-6343-0217
Jidong Wang: 0000-0001-9110-6799

Notes

The authors declare no competing financial interest.

■ REFERENCES

(1) Ohara, T.; Sato, T.; Shimizu, N.; Prescher, G.; Schwind, H.; Weiberg, O.; Marten, K.; Greim, H., Acrylic Acid and Derivatives. In *Ullmann's Encyclopedia of Industrial Chemistry*; Wiley-VCH, 2000.

(2) Vitcha, J. F.; Sims, V. A. Vapor Phase Aldol Reaction. Acrylic Acid by Reaction of Acetic Acid and Formaldehyde. *Ind. Eng. Chem. Prod. Res. Dev.* **1966**, *5*, 50−53.

(3) Fernholz, H.; Wunder, F. A process for the preparation of methyl acrylate by oxidation of methyl acetate or a mixture of methyl acetate and methanol. D.E. Patent 1,294,956, May 14, 1969.

(4) Ai, M. Vapor-phase aldol condensation of formaldehyde with acetic acid on V_2O_5-P_2O_5 catalysts. *J. Catal.* **1987**, *107*, 201−208.

(5) Ai, M. Vapor-phase aldol condensation of formaldehyde with propionic acid on vanadium pentoxide—phosphorus pentoxide. *Appl. Catal.* **1988**, *36*, 221−230.

DOI: 10.1021/acs.iecr.7b02841
Ind. Eng. Chem. Res. 2018, 57, 2773−2786

(6) Ai, M. Effect of the composition of vanadium-titanium binary phosphate on catalytic performance in vapor-phase aldol condensation. *Appl. Catal.* **1989**, *54*, 29−36.

(7) Ai, M. Reaction of acetic acid with methanol over vanadium-titanium binary phosphate catalysts in the presence of oxygen. *Appl. Catal.* **1990**, *59*, 227−235.

(8) Ai, M. The effects of the reaction variables on the yields of acrylic acid and methyl acrylate in the reaction of acetic acid with methanol in the presence of oxygen. *Bull. Chem. Soc. Jpn.* **1990**, *63*, 199−202.

(9) Feng, X. Z.; Sun, B.; Yao, Y.; Su, Q.; Ji, W. J.; Au, C. T. Renewable production of acrylic acid and its derivative: New insights into the aldol condensation route over the vanadium phosphorus oxides. *J. Catal.* **2014**, *314*, 132−141.

(10) Ai, M. Formation of methyl methacrylate by condensation of methyl propionate with formaldehyde over silica-supported cesium hydroxide catalysts. *Appl. Catal., A* **2005**, *288*, 211−215.

(11) Li, B.; Yan, R. Y.; Wang, L.; Diao, Y. Y.; Li, Z. X.; Zhang, S. J. SBA-15 supported cesium catalyst for methyl methacrylate synthesis via condensation of methyl propionate with formaldehyde. *Ind. Eng. Chem. Res.* **2014**, *53*, 1386−1394.

(12) Yan, J. B.; Zhang, C. L.; Ning, C. L.; Tang, Y.; Zhang, Y.; Chen, L. L.; Gao, S.; Wang, Z. L.; Zhang, W. X. Vapor phase condensation of methyl acetate with formaldehyde to preparing methyl acrylate over cesium supported SBA-15 catalyst. *J. Ind. Eng. Chem.* **2015**, *25*, 344−351.

(13) Wang, Y. A.; Yan, R. Y.; Lv, Z. P.; Wang, H.; Wang, L.; Li, Z. X.; Zhang, S. J. Lanthanum and cesium-loaded SBA-15 catalysts for MMA synthesis by aldol condensation of methyl propionate and formaldehyde. *Catal. Lett.* **2016**, *146*, 1808−1818.

(14) Dumitriu, E.; Hulea, V.; Chelaru, C.; Catrinescu, C.; Tichit, D.; Durand, R. Influence of the acid−base properties of solid catalysts derived from hydrotalcite-like compounds on the condensation of formaldehyde and acetaldehyde. *Appl. Catal., A* **1999**, *178*, 145−157.

(15) Dumitriu, E.; Hulea, V.; Fechete, I.; Auroux, A.; Lacaze, J.-F.; Guimon, C. The aldol condensation of lower aldehydes over MFI zeolites with different acidic properties. *Microporous Mesoporous Mater.* **2001**, *43*, 341−359.

(16) He, D.; Huang, W.; Liu, J.; Zhu, Q. The activity of $H_4SiW_{12}O_{40}$ for the coupling of formaldehyde and methyl formate to methyl glycolate and methyl methoxy acetate. *J. Mol. Catal. A: Chem.* **1999**, *145*, 335−338.

(17) Wang, G.; Li, Z.; Li, C.; Wang, H. Kinetic and thermodynamic studies on one-step synthesis of methyl acrylate promoted by generated ionic liquid at mild temperature. *Chem. Eng. J.* **2017**, *319*, 297−306.

(18) Zhang, G. L.; Zhang, H. H.; Yang, D.; Li, C. S.; Peng, Z. J.; Zhang, S. J. Catalysts, kinetics and process optimization for the synthesis of methyl acrylate over Cs-P/γ-Al_2O_3. *Catal. Sci. Technol.* **2016**, *6*, 6417−6430.

(19) Yang, D.; Li, D.; Yao, H.; Zhang, G.; Jiao, T.; Li, Z.; Li, C.; Zhang, S. Reaction of formalin with acetic acid over vanadium−phosphorus oxide bifunctional catalyst. *Ind. Eng. Chem. Res.* **2015**, *54*, 6865−6873.

(20) Yang, D.; Sararuk, C.; Suzuki, K.; Li, Z. X.; Li, C. S. Effect of calcination temperature on the catalytic activity of VPO for aldol condensation of acetic acid and formalin. *Chem. Eng. J.* **2016**, *300*, 160−168.

(21) Hu, J.; Lu, Z.; Yin, H.; Xue, W.; Wang, A.; Shen, L.; Liu, S. Aldol condensation of acetic acid with formaldehyde to acrylic acid over SiO_2-, SBA-15-, and HZSM-5-supported V-P-O catalysts. *J. Ind. Eng. Chem.* **2016**, *40*, 145−151.

(22) Cano, L. A.; Cagnoli, M. V.; Bengoa, J. F.; Garcia-Fierro, J. L.; Marchetti, S. G. Synthesis and characterization of SBA-15 modified with alkali metals. *J. Porous Mater.* **2017**, *24*, 631−638.

(23) Díez, V. K.; Apesteguía, C. R.; Di Cosimo, J. I. Acid−base properties and active site requirements for elimination reactions on alkali-promoted MgO catalysts. *Catal. Today* **2000**, *63*, 53−62.

(24) Bal, R.; Tope, B.; Das, T.; Hegde, S.; Sivasanker, S. Alkali-loaded silica, a solid base: investigation by FTIR spectroscopy of adsorbed CO_2 and its catalytic activity. *J. Catal.* **2001**, *204*, 358−363.

(25) Käßner, P.; Baerns, M. Comparative characterization of basicity and acidity of metal oxide catalysts for the oxidative coupling of methane by different methods. *Appl. Catal., A* **1996**, *139*, 107−129.

(26) Hochgreb, S.; Dryer, F. Decomposition of 1, 3, 5-trioxane at 700−800 K. *J. Phys. Chem.* **1992**, *96*, 295−297.

(27) Wang, Z. X.; Wang, D. X.; Zhao, Z.; Chen, Y.; Lan, J. A DFT study of the structural units in SBA-15 mesoporous molecular sieve. *Comput. Theor. Chem.* **2011**, *963*, 403−411.

(28) Frisch, M. J.; Trucks, G. W.; Schlegel, H. B.; Scuseria, G. E.; Robb, M. A.; Cheeseman, J. R.; Scalmani, G.; Barone, V.; Mennucci, B.; Petersson, G. A.; Nakatsuji, H.; Caricato, M.; Li, X.; Hratchian, H. P.; Izmaylov, A. F.; Bloino, J.; Zheng, G.; Sonnenberg, J. L.; Hada, M.; Ehara, M.; Toyota, K.; Fukuda, R.; Hasegawa, J.; Ishida, M.; Nakajima, T.; Honda, Y.; Kitao, O.; Nakai, H.; Vreven, T.; Montgomery, J. A., Jr.; Peralta, J. E.; Ogliaro, F.; Bearpark, M.; Heyd, J. J.; Brothers, E.; Kudin, K. N.; Staroverov, V. N.; Kobayashi, R.; Normand, J.; Raghavachari, K.; Rendell, A.; Burant, J. C.; Iyengar, S. S.; Tomasi, J.; Cossi, M.; Rega, N.; Millam, J. M.; Klene, M.; Knox, J. E.; Cross, J. B.; Bakken, V.; Adamo, C.; Jaramillo, J.; Gomperts, R.; Stratmann, R. E.; Yazyev, O.; Austin, A. J.; Cammi, R.; Pomelli, C.; Ochterski, J. W.; Martin, R. L.; Morokuma, K.; Zakrzewski, V. G.; Voth, G. A.; Salvador, P.; Dannenberg, J. J.; Dapprich, S.; Daniels, A. D.; Farkas, O.; Foresman, J. B.; Ortiz, J. V.; Cioslowski, J.; Fox, D. J. *Gaussian 09*, revision A.01; Gaussian, Inc.: Wallingford CT, 2009.

(29) Lu, T.; Chen, F. Multiwfn: a multifunctional wavefunction analyzer. *J. Comput. Chem.* **2012**, *33*, 580−92.

(30) Humphrey, W.; Dalke, A.; Schulten, K. VMD: Visual molecular dynamics. *J. Mol. Graphics* **1996**, *14*, 33−38.

(31) Stephens, P. J.; Devlin, F. J.; Chabalowski, C. F.; Frisch, M. J. Ab initio calculation of vibrational absorption and circular dichroism spectra using density functional force fields. *J. Phys. Chem.* **1994**, *98*, 11623−11627.

(32) Lu, Q.; Wang, Z.; Li, J.; Wang, P.; Ye, X. Structure and photoluminescent properties of ZnO encapsulated in mesoporous silica SBA-15 fabricated by two-solvent strategy. *Nanoscale Res. Lett.* **2009**, *4*, 646−54.

(33) Wang, X.; Sun, T.; Yang, J.; Zhao, L.; Jia, J. Low-temperature H_2S removal from gas streams with SBA-15 supported ZnO nanoparticles. *Chem. Eng. J.* **2008**, *142*, 48−55.

(34) El-Nahhal, I. M.; Salem, J. K.; Selmane, M.; Kodeh, F. S.; Ebtihan, H. A. Synthesis and structural characterization of ZnO and CuO nanoparticles supported mesoporous silica SBA-15. *Chem. Phys. Lett.* **2017**, *667*, 165−171.

(35) Tai, J.; Davis, R. J. Synthesis of methacrylic acid by aldol condensation of propionic acid with formaldehyde over acid−base bifunctional catalysts. *Catal. Today* **2007**, *123*, 42−49.

(36) Gogate, M. R.; Spivey, J. J.; Zoeller, J. R. Synthesis of methyl methacrylate by vapor phase condensation of formaldehyde with propionate derivatives. *Catal. Today* **1997**, *36*, 243−254.

(37) Sharma, R. V.; Soni, K. K.; Dalai, A. K. Preparation, characterization and application of sulfated Ti-SBA-15 catalyst for oxidation of benzyl alcohol to benzaldehyde. *Catal. Commun.* **2012**, *29*, 87−91.

(38) Yuan, P.; Wu, D. Q.; He, H. P.; Lin, Z. Y. The hydroxyl species and acid sites on diatomite surface: a combined IR and Raman study. *Appl. Surf. Sci.* **2004**, *227*, 30−39.

(39) Bukallah, S. B.; Bumajdad, A.; Khalil, K. M. S.; Zaki, M. I. Characterization of mesoporous VOx/MCM-41 composite materials obtained via post-synthesis impregnation. *Appl. Surf. Sci.* **2010**, *256*, 6179−6185.

(40) Podgornov, E. A.; Prosvirin, I. P.; Bukhtiyarov, V. I. , XPS, TPD and TPR studies of Cs−O complexes on silver: their role in ethylene epoxidation. *J. Mol. Catal. A: Chem.* **2000**, *158*, 337−343.

(41) Bukhtiyarov, V. I.; Prosvirin, I. P.; Kvon, R. I.; Bal'zhinimaev, B. S.; Podgornov, E. A. XPS and TPD studies of Cs-O complexes on Ag

DOI: 10.1021/acs.iecr.7b02841
Ind. Eng. Chem. Res. 2018, 57, 2773−2786

surfaces: single crystal versus supported catalysts. *Appl. Surf. Sci.* **1997**, *115*, 135−143.
(42) Phillips, C. C.; Hughes, A. E.; Sibbett, W. Quantitative XPS analysis of the chemical composition of S1(Ag-O-Cs) photocathodes and its relation to the photosensitivity. *J. Phys. D: Appl. Phys.* **1984**, *17*, 611.
(43) Wang, X.; Lin, K. S.; Chan, J. C.; Cheng, S. Direct synthesis and catalytic applications of ordered large pore aminopropyl-functionalized SBA-15 mesoporous materials. *J. Phys. Chem. B* **2005**, *109*, 1763−9.
(44) Chen, Y.; Han, J.; Zhang, H. Structure and acid−base properties of surface-modified mesoporous silica. *Appl. Surf. Sci.* **2007**, *253*, 9400−9406.
(45) Guo, X.; Yang, D.; Zuo, C.; Peng, Z.; Li, C.; Zhang, S. Catalysts, process optimization, and kinetics for the production of methyl acrylate over vanadium phosphorus oxide catalysts. *Ind. Eng. Chem. Res.* **2017**, *56*, 5860−5871.
(46) Bao, Q.; Bu, T.; Yan, J.; Zhang, C.; Ning, C.; Zhang, Y.; Hao, M.; Zhang, W.; Wang, Z. Synthesis of methyl acrylate by aldol condensation of methyl acetate with formaldehyde over Al_2O_3-supported barium catalyst. *Catal. Lett.* **2017**, *147*, 1540−1550.
(47) Sararuk, C.; Yang, D.; Zhang, G.; Li, C.; Zhang, S. One-step aldol condensation of ethyl acetate with formaldehyde over Ce and P modified cesium supported alumina catalyst. *J. Ind. Eng. Chem.* **2017**, *46*, 342−349.
(48) Yang, F.; Hou, Y.; Wu, W.; Wang, Q.; Niu, M.; Ren, S. The relationship between benzene carboxylic acids from coal via selective oxidation and coal rank. *Fuel Process. Technol.* **2017**, *160*, 207−215.
(49) Liu, B.; Wang, D.; Wang, Z.; Zhao, Z.; Chen, Y.; Lan, J. The structure and activity of potassium supported on SBA-15 molecular sieve: Density functional theory study. *J. Theor. Comput. Chem.* **2014**, *13*, 1350076.
(50) Manzetti, S.; Lu, T. The geometry and electronic structure of Aristolochic acid: possible implications for a frozen resonance. *J. Phys. Org. Chem.* **2013**, *26*, 473−483.
(51) Murray, J. S.; Concha, M. C.; Politzer, P. Molecular surface electrostatic potentials as guides to Si-O-N angle contraction: tunable σ-holes. *J. Mol. Model.* **2011**, *17*, 2151−7.

DOI: 10.1021/acs.iecr.7b02841
Ind. Eng. Chem. Res. 2018, 57, 2773−2786